Contract Report

High Throughput, Low Toxic Processing of Very Thin, High Efficiency CIGSS Solar Cells

NREL contract no. XXL-5-44205-08, UCF/FSEC Account no. 2012 8098

Year 2, Annual Report

Report no. FSEC-CR-1707-19

May 22, 2007

Prepared for

National Renewable Energy Laboratory
1617 Cole Boulevard
Golden, CO 80401

Submitted by

Neelkanth G. Dhere
Florida Solar Energy Center®
1679 Clearlake Road
Cocoa, FL 32922-5703

TABLE OF CONTENTS

1: INTRODUCTION 3

2: OPTIMIZATION OF METALLIC PRECURSOR DEPOSITION AND SELENIZATION/SULFURIZATION IN THE CONVENTIONAL FURNACE FOR CIGSeS .. 4

3: RAPID THERMAL PROCESSING 13

4. CIGS2 THIN FILM SOLAR CELLS 21

5. ZnCdS AND ZnS AS ALTERNATIVE BUFFER LAYER FOR CIGS2 SOLAR CELLS 24

6. ULTRA THIN CIGS/CIGSS ABSORBER LAYER 29

7. MAINTENANCE AND REPAIR OF VACUUM SYSTEMS 31

8. REFERENCES 33

1: INTRODUCTION

The major concern in the photovoltaic industry is to reduce the cost of PV modules below $1.00/peak watt so as to make the technology economically viable. The research activities at the FSEC PV Materials Lab are focused on developing highly efficient thin-film solar cells capable of being produced using an economical process for achieving this goal. $CuIn_{1-x}Ga_xSe_{2-y}S_y$ (CIGSeS) is a potential candidate for this purpose. Sputtering is the technique capable of providing high yield and high production volume. Research activities presented here focuses on developing CIGSeS thin films by depositing elemental precursor Cu-In-Ga by magnetron sputtering technique followed by selenization/sulfurization in either conventional furnace or by rapid thermal processing. During the first year, experiments were carried out to optimize conditions for both conventional and rapid thermal processing approaches. Also experiments were conducted on very thin absorber layers with both the conventional and rapid thermal processing approaches. These initial experiments towards optimizing the selenization parameters were discussed in detail in earlier reports.

2: OPTIMIZATION OF METALLIC PRECURSOR DEPOSITION AND SELENIZATION/SULFURIZATION IN THE CONVENTIONAL FURNACE FOR CIGSeS

Earlier, PV Mat Lab at the Florida Solar Energy Center achieved record efficiency of 13.73% on CIGSeS thin film solar cell on small area by the sputtering-conventional furnace. After achieving the highest efficiency experiments were carried out to improve the material quality to further increase the efficiency. A detailed study is being carried out by varying the process parameters.

Experimentation:

Optimization of the process parameters was carried out. In the earlier samples the Cu/(In+Ga) ratio was lower than the desired value of 0.92. The sputtering rates for CuGa and In calibrated earlier with the respective sputtering powers and argon pressures were maintained. CuGa content was kept constant by keeping the substrate movement speed constant for all CuGa depositions. Cu/(In+Ga) ratio was systematically increased by reducing the indium content, i.e. by increasing the substrate movement speeds over the indium target while keeping the deposition rate constant. Three different indium contents 1. high, 2. intermediate (9% less) and 3. low (16% less) corresponding to low, intermediate, and high substrate movement speeds were chosen. The Cu/(In+Ga) ratio for the absorber prepared with intermediate indium deposition timing was ~1. Hence an average of the intermediate and high indium deposition timing was selected.

Sodium available during growth of CIGS is known to influence the growth kinetics, leading to structurally and electronically modified absorber material. Substrates for the CIGS / CIGSeS thin film fabrication were chosen with and without the alkali barrier. This was done to study the effect of sodium on the film growth. Sodium containing precursor, NaF film was deposited prior to the precursor deposition on the molybdenum coated substrate with an alkali barrier. Three different thicknesses of NaF, viz. 40 Å, 80 Å and 120 Å were deposited. Mo-coated glass without the alkali barrier layer was used as a substrate to determine the amount of sodium out diffusion from the substrate was adequate to enhance the material- as well as the electronic properties. 40 Å and 80 Å thick layers of NaF were also deposited on the SLG substrate without the alkali barrier.

The CIGS / CIGSeS thin film absorbers were prepared using a two stage process. Stage one involved the deposition of CuGa-In metallic precursors on molybdenum coated sodalime glass substrate. Stage two involved the selenization and sulfurization of the metallic precursors in the DESe and H_2S ambient respectively. The entire elemental stack was selenized or selenized and sulfurized in the temperature range of 475 ºC - 515 ºC. Parameters have been optimized to achieve better control during the selenization/sulfurization process. New robust thermocouples were installed to monitor the process temperature. Highly efficient ultra-thin solar cell is the ultimate goal of this research. After achieving films (2.5 – 2.7 μm) with good morphology process have been optimized to fabricate 1.8 – 2.0 μm thin film.

Electron probe microanalysis (EPMA) at NREL and x-ray energy dispersive spectroscopy (XEDS) analysis at MCF were carried out to study the chemical composition of the film. Optical microscopy (FSEC), scanning electron microscopy (SEM) at MCF and atomic force microscopy (AFM) at NREL were carried out to study the morphology of the film. XRD

analysis was carried to study the crystal structure and phases. Quantum efficiency (QE), capacitance–voltage (C-V) and light beam induced current (LBIC) measurement of the champion cell were carried out.

Results and Discussion:

Composition

The atomic concentrations of the elements Cu, In, Ga, Se and S and Cu/In+Ga ratios for CIGSeS thin film with varying indium quantity are shown in the Table I. The compositions analyzed by EPMA using electron beam energies of 10 kV and 20 kV correspond respectively to the near the surface of the film and bulk of the film. As can be seen from Table I, Cu/In+Ga ratios for the high indium content are in the range 0.76 – 0.83. As can be seen the films tend to become copper-rich with intermediate and low indium deposition times. Hence an average indium deposition time between high and intermediate was chosen. The Cu/In+Ga ratio for the 2 μm thick absorber is 0.87.

Experiments were also carried out to optimize the selenization and sulfurization timings. For the initial experiments the S/(Se+S) ratio was 0.032–0.062. In the subsequent experiments, selenization time was reduced while increasing the sulfurization time. Consequently significantly higher S/(Se+S) ratios in the range 0.213-0.287 were obtained.

Table I: Chemical composition CIGSeS absorbers with varying indium content as analyzed by EPMA at 10 kV and 20 kV e-beam energy

ID	Indium	Voltage	Cu	In	Ga	Se	S
VK1	High	10 kV	23.07	26.67	1.02	46.37	2.88
VK1	High	20 kV	22.13	24.86	3.38	47.45	2.18
N3b	Intermediate	10 kV	25.78	22.16	3.51	34.66	13.89
N3b	Intermediate	20 kV	25.33	20.32	5.13	36.53	12.70
N4b	Low	10 kV	26.51	21.93	3.01	34.60	13.95
N4b	Low	20 kV	25.96	20.54	4.85	37.69	10.96
617C8A	Avg	10 kV	23.16	25.78	1.46	30.72	18.85
617C8A	Avg	20 kV	23.77	24.55	3.02	38.19	10.98

X-ray Energy Dispersive Spectroscopy

XEDS analysis was also carried out to cross verify the EPMA results (Figure 1). XEDS results shows that the composition was almost the same with the medium indium deposition timing.

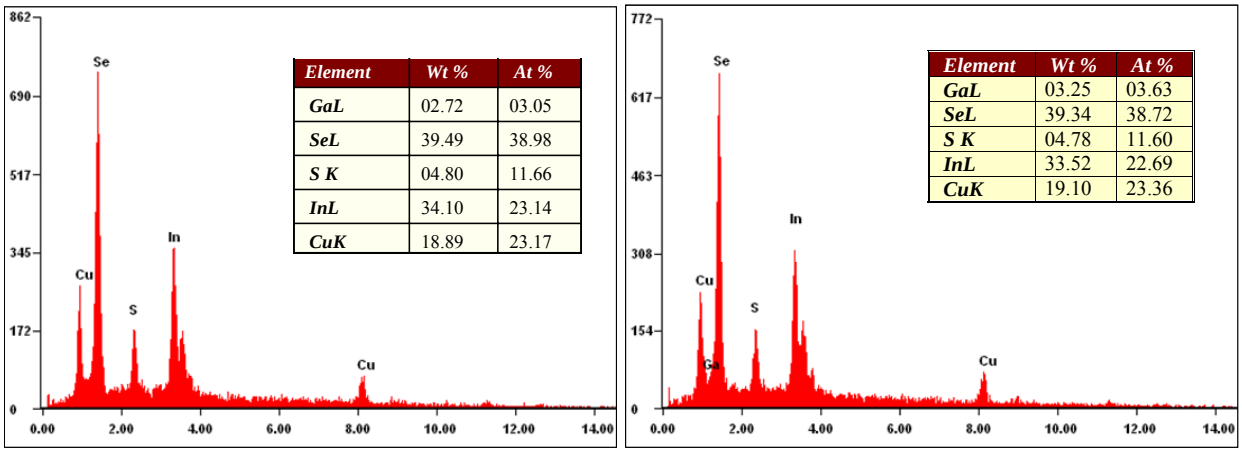

Figure 1: XEDS Analysis of CIGSeS

Morphology:

Both optical and SEM micrographs indicate that the grains are packed compactly. The CIGSeS thin films on sodalime glass (SLG) with the barrier were selenized and sulfurized at 515 ºC. CIGSeS thin film with 120 Å NaF had large grains (Figure 3A) compared to the one with 40 Å NaF (Figure 3B). This may be attributed to the quantity of sodium in the film. The CIGS thin films on SLG without the barrier were selenized at 475 ºC. Both films with no additional NaF (Figure 4A) and 40 Å NaF (Figure 4B) show compact grain structure. But the sample with no additional NaF has uneven grains whereas the sample with 40 Å NaF shows better morphology with large grains. The uneven grains (Figure 4A) may be due to uneven sodium out diffusion from the SLG. Comparing (Figure 4A and 4B) it can be said that the addition of optimal amount NaF tends to improve the morphology. All the films show well faceted grains. But the films selenized and sulfurized at 515 ºC show higher amount of faceting compared to the film selenized at 475 ºC. This effect is due to higher process temperature. The cross sectional SEM of the CIGS thin film selenized at 475 ºC show better columnar grains in case of the film with additional 40 Å NaF (Figure 5A) when compared to film with no additional NaF (Figure 5B).

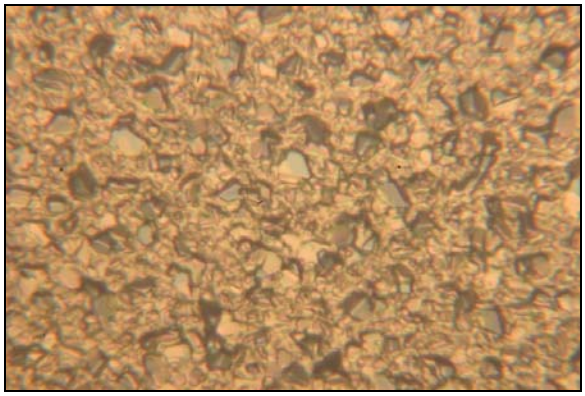

Figure 2: Optical micrograph (x500) of the CIGS thin film on SLG, selenized at 475 ºC.

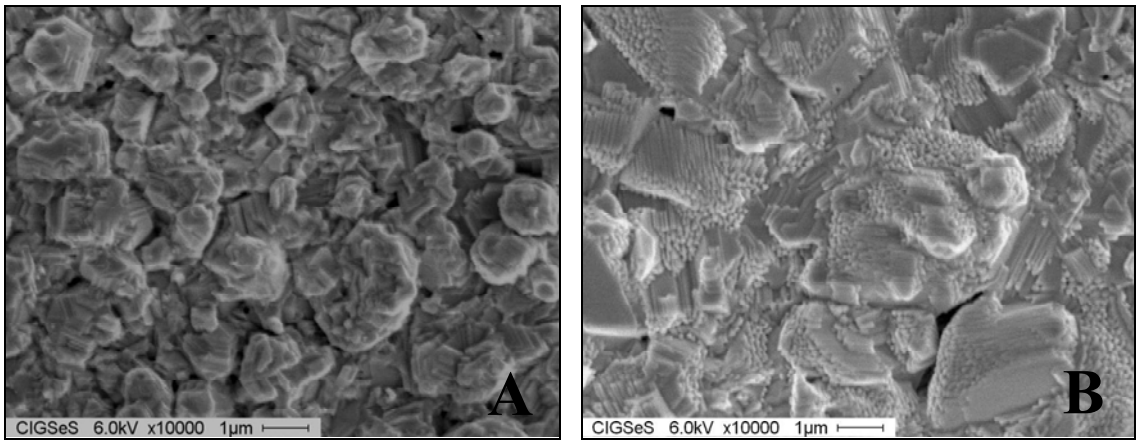

Figure 3: SEM micrograph of the CIGSeS film on SLG with an alkali barrier having (**A**) 40 Å and (**B**) 120 Å layer of NaF and selenized and sulfurized at 515 ºC (2.5 – 2.7 µm).

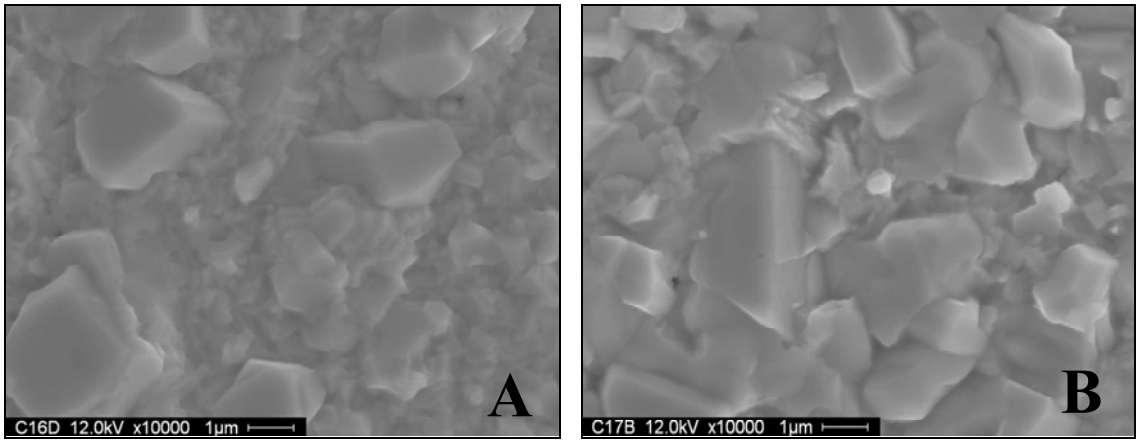

Figure 4: SEM micrograph of the CIGS film on SLG without the alkali barrier having (**A**) no NaF and (**B**) 40 Å layer of additional NaF and selenized at 475 ºC (1.8 – 2.0).

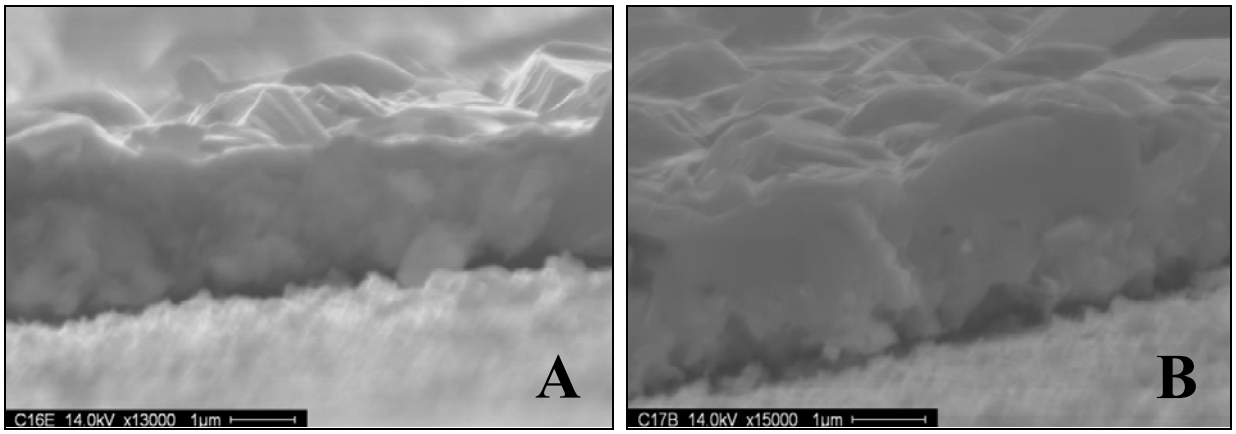

Figure 5: Cross sectional SEM micrograph of the CIGS film on SLG without the alkali barrier having (**A**) no NaF and (**B**) 40 Å NaF and selenized at 475 ºC (1.8 – 2.0).

Figure 6 (A and B) show the 2D and 3D AFM micrographs respectively of the CIGSeS thin film selenized/sulfurized at 515 °C. This film was fabricated on SLG with an alkali barrier with 120 Å NaF. Figure 6 (A and B) also show that the film has compact morphology and grain distribution. The average roughness, R_a of the film was 142 nm. 3D micrograph reveals the formation of islands and the grains. Figure 6B also reveals the formation of facets due to the higher process temperature. Due to better process control and optimization of parameters the average roughness has been reduced to 50 – 70 nm. The average roughness is measured using the surface profilometer.

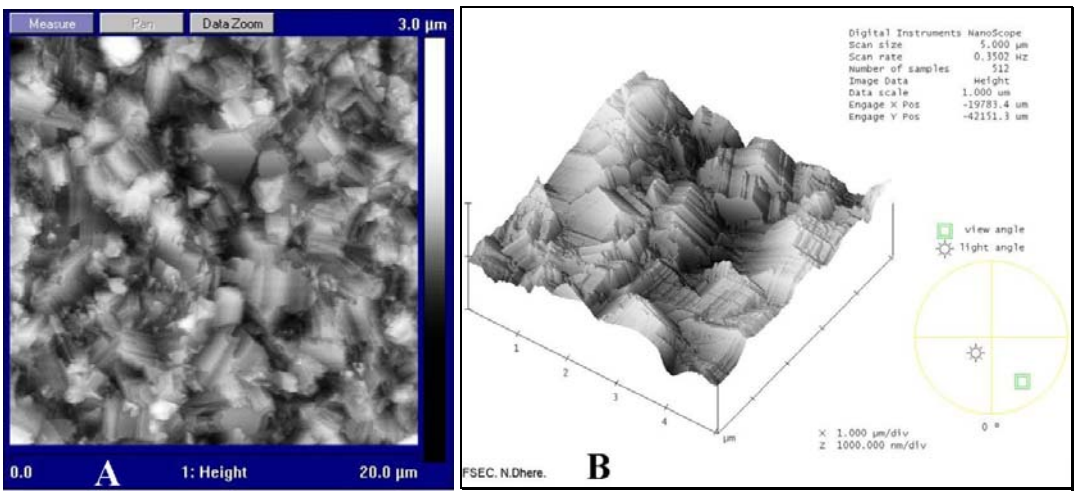

Figure 6: AFM 2D micrograph (A) and 3D micrograph (B) of CIGSeS thin film selenized sulfurized at 515 °C.

X - Ray Diffraction Analysis

X-ray diffraction pattern (Figure 7) of 2 µm thick absorber show the growth of chalcopyrite phase of CIGS with the (112) preferred orientation. The lattice parameters are a= 5.778 Å and c= 11.558 Å. XRD pattern for a sample selenized at 475ºC show (101), (112), (103), (204/220), and (116/312) reflections from $CuIn_{0.9}Ga_{0.1}Se_2$ phase.

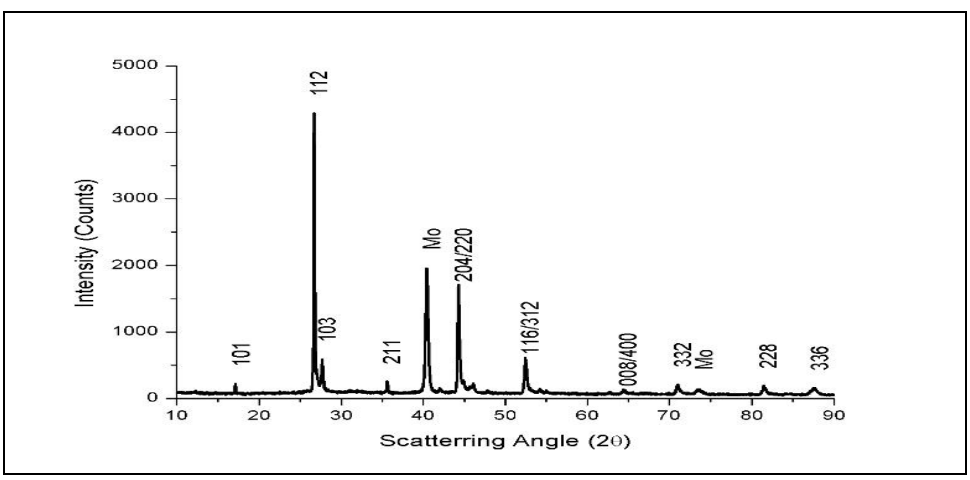

Figure 7: XRD pattern of CIGSeS ~2 µm thick absorber

Figure 8 shows the XRD diffraction pattern of the CIGS/Mo/SLG structure with no alkali barrier. The red and blue colored plots correspond to sample with no sodium fluoride and with 40 Å of additional NaF. The amount of sodium out-diffusion from the SLG is yet to be studied. Sodium in the CIGS and /or Mo layer aids in the formation of $MoSe_2$ at the CIGS/Mo interface during the CIGS formation [1]. Increase in sodium quantity during the CIGS formation reduces the formation of $MoSe_2$ [2]. In Figure 8, the preferred orientation (002) peak of $MoSe_2$ can be clearly seen for both the films. But the intensity reduces with the increase in sodium quantity. Similarly the preferential growth of $MoSe_2$ in (100) and (110) is suppressed when the quantity of sodium increases (Figure 8). The preferential growth of $MoSe_2$ in (100) and (110) may facilitate the diffusion of Se through the already formed $MoSe_2$, thus leading to larger $MoSe_2$ thickness [2]. Hence we can conclude that the thickness of $MoSe_2$ is not excessive. A detailed TEM analysis will be carried out to check the $MoSe_2$ thickness.

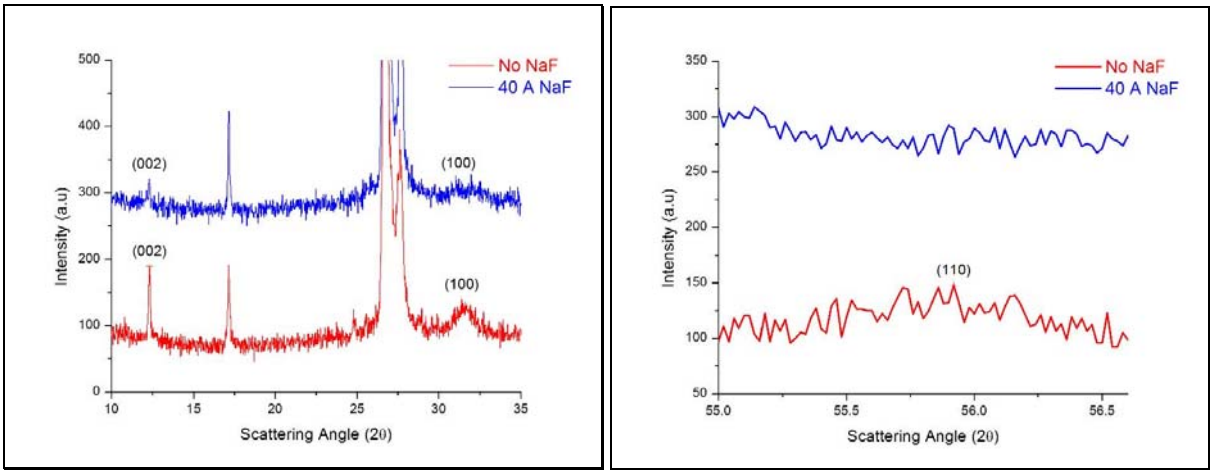

Figure 8: XRD diffraction pattern of CIGS/MO/SLG

CIGSeS Champion Cell Analysis:

The CIGSeS champion cell with efficiency of 13.73 showed a different pattern near the red response in the quantum efficiency (QE) measurement (Figure 9A). A QE measurement of an adjacent cell was again carried out at Colorado State University (CSU) by Dr. Sites group and the results were confirmed to be same (Figure 9B). The bandgap appears to be near 1.0 eV i.e., very close to that of $CuInSe_2$.

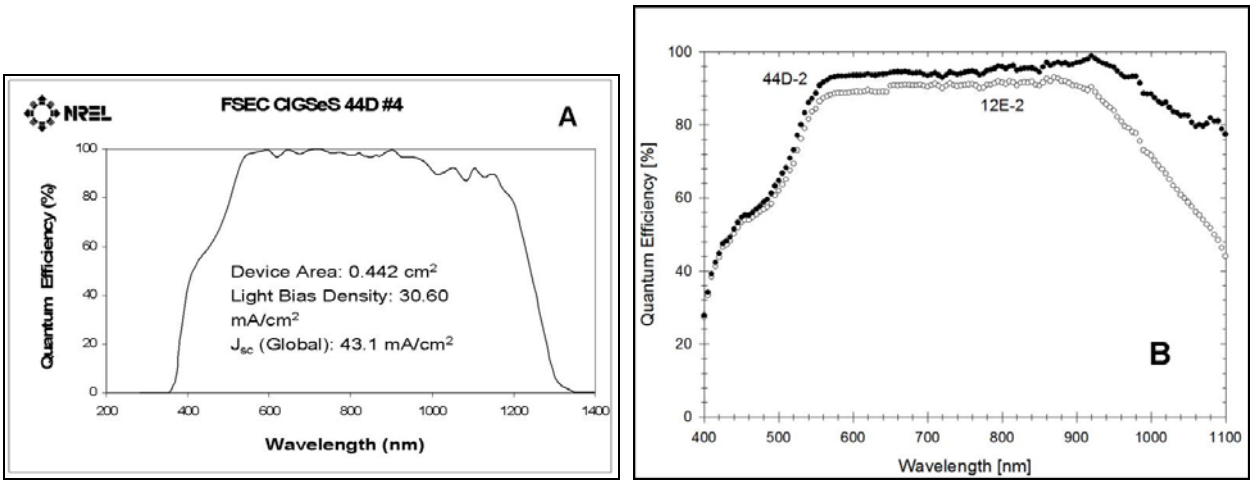

Figure 9: Internal Quantum efficiency measurement at NREL (A) and external quantum efficiency measurement at CSU (B)

Capacitance – Voltage Measurements:

Capacitance – Voltage (C-V) measurements were also carried out on the champion cell array (Figure 10). As seen from the given plot the data points are consistent and the C^{-2} vs V plots are reasonably linear with plausible voltage intercepts. The inferred hole concentration are all in the mid 10^{14} range with modest variation between cells on the same substrate.

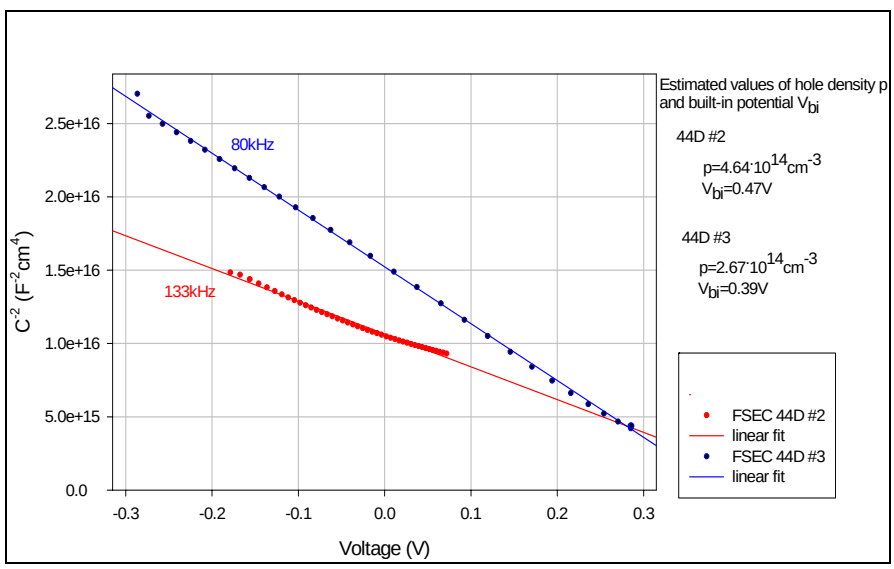

Figure 10: C-V Measurement

Light Beam Induced Current:

LBIC is a reliable tool for investigating a variety of solar cell non-uniformities. Figure 11 shows the LBIC photoresponse (QE) maps for the one shunted (A) and one non-shunted (B). Part of the dark area at the top is the probe shadow, and there seems to be a bad bottom left corner (Figure 11A). The absolute QE is not calibrated, but it is clearly a factor of 10 to 20 less for the shunted cells. The shunted pattern spreads gradually over the entire cell. The variation in the QE is in the range of 61-66% for the shunted cell and for the non shunted is in the range of 0-5%.

Three standard resolutions have been used for LBIC measurements (Figure 12). The lowest resolution has a 5 mm by 10 mm field with a 100 μm spot (A). This resolution covers the whole portion of the cell. The small square (A) in this view is magnified ten times for 500 by 500 μm field and a 10 μm spot. The area shown in that map's small square (1) is multiplied 10 times more for the 50 by 50 μm field with a 1 μm spot for the high resolution map. The probe intensity is held near one sun for all of the LBIC measurements. This process makes it straightforward to zoom in on a small area of particular interest and to return to the same area even after the cell has been removed from the apparatus for other measurements. A quantum-efficiency change of 5% (61-66%) is observed. The sample may have been damaged during the extensive transport and considerable handling.

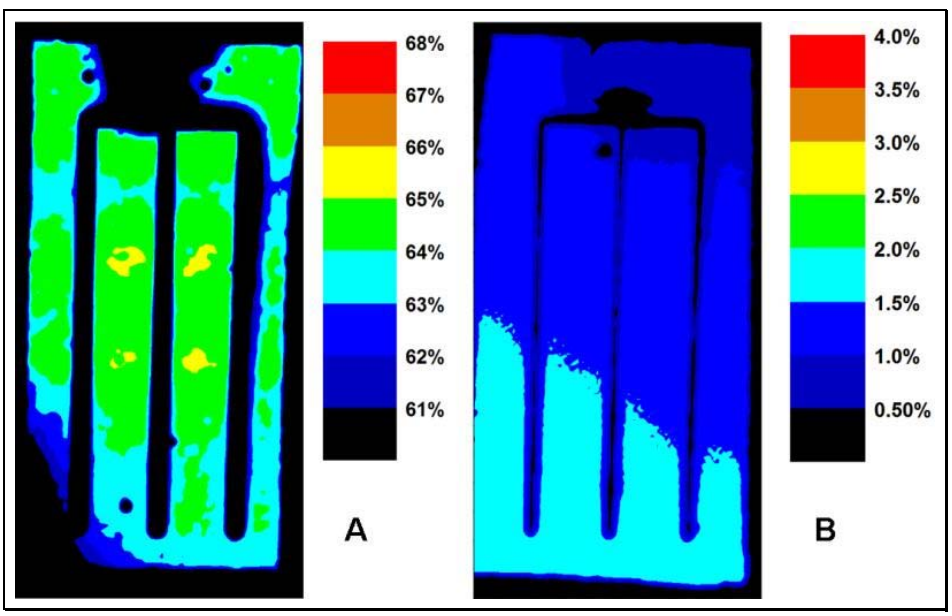

Figure 11: LBIC photoresponse (QE) maps A: Non-shunted B: Shunted

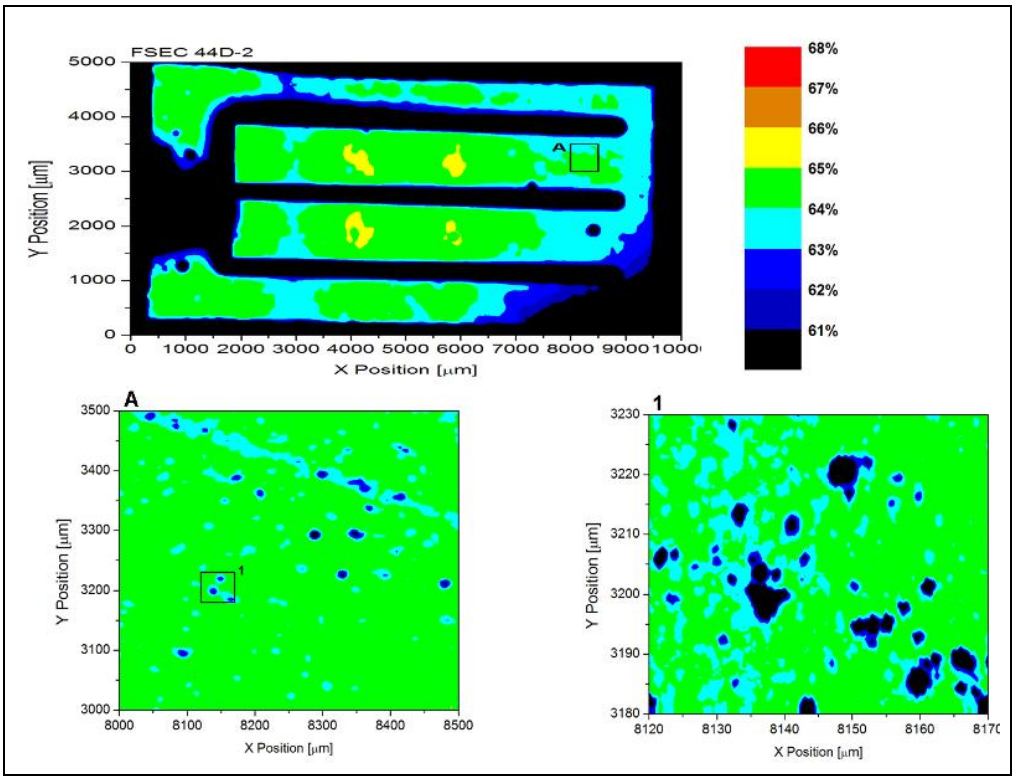

Figure 12: LBIC with low, mid and high resolution (100 µm, 10 µm, and 1 µm spots).

3: RAPID THERMAL PROCESSING

Rapid thermal processing (RTP) provides a way to rapidly heat substrates to an elevated temperature. After getting encouraging results during research carried out in the first year, (efficiencies approaching 13%) [3] Further optimization of the RTP process is being carried out. Currently experiments are done to optimize the Cu/In+Ga ratio. Experiments are also done to optimize the sodium content. During CuGa and indium sputtering, substrate movement speed was kept at 50 seconds/1" and 82.5 seconds/1" respectively. The detailed material and photovoltaic characterization is being carried out by EPMA, XEDS, XRD, SEM, TEM, I-V and QE techniques.

Composition:

The EPMA results of the CIGSeS samples are given in following Table II. Letters U and E at the end of the sample identification number correspond to unetched and etched absorber films respectively. The Cu/In+Ga ratio (for unetched samples) near the surface is ~ 0.84 to 0.92 and in the bulk for unetched samples is ~0.82 to 0.84.

Table II: EPMA analysis for CIGSeS sample fabricated by RTP.

Sample ID	NaF (Å)	Voltage (kV)	Cu	In	Ga	Se	S	Cu/In+Ga	S/Se+S
SK16U	120	10	23.37	26.20	1.49	27.80	21.14	0.84	0.43
SK16U	120	20	22.73	24.24	3.61	30.84	18.57	0.82	0.38
SK17U	80	10	24.62	25.49	1.17	34.98	13.73	0.92	0.28
SK17U	80	20	23.04	24.00	3.53	36.47	12.97	0.84	0.26
SK16E	120	10	23.19	26.75	1.20	25.86	23.01	0.83	0.47
SK16E	120	20	22.14	24.56	3.82	28.37	21.11	0.78	0.42
SK17E	80	10	23.39	26.31	1.26	29.49	19.56	0.85	0.40
SK17E	80	20	22.89	24.39	3.44	31.32	17.96	0.82	0.36

Morphology:

Following images show AFM analysis of CIGSeS samples fabricated by RTP.

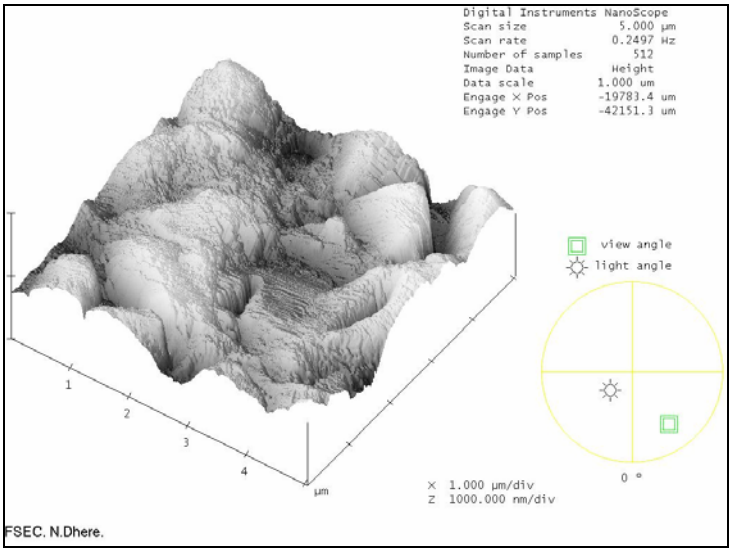

Figure 13: AFM 3D surface topography of CIGSeS thin film (Sample SK16E)

AFM three dimensional CIGSeS sample surface topography is shown in figure 13. Grain size of ~1 to 2 microns can be seen. RTP films usually have comparatively smaller grains as the time for film formation is low.

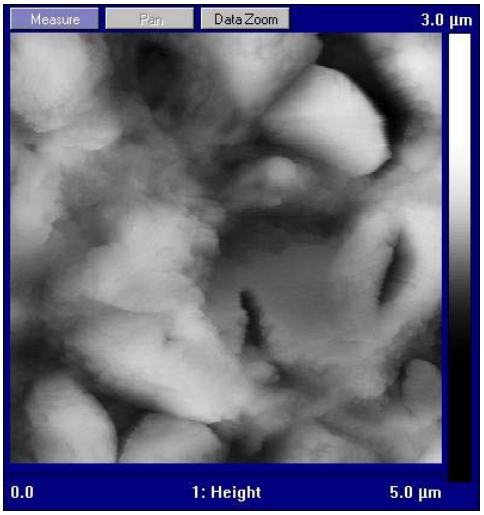

Figure 14: AFM 2D image of CIGSeS thin film (Sample SK16E)

AFM surface image of the surface of CIGSeS sample prepared by RTP is shown in figure 14. Compactly packed grains with hillocks and valleys can be seen from AFM images. Further experimentation and characterization is being carried out.

Experiments were carried out using molybdenum coated sodalime glass substrates without sodium-diffusion barrier layer. In the earlier experiments, molybdenum coated sodalime glass substrates with sodium-diffusion barrier layer were used.

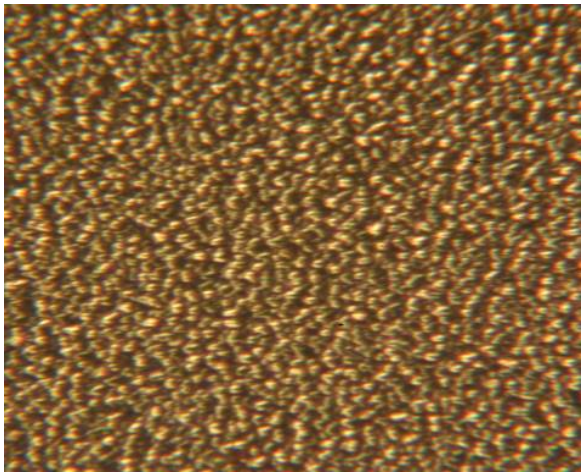

Figure 15: CIGSeS high magnification (1317R21A)

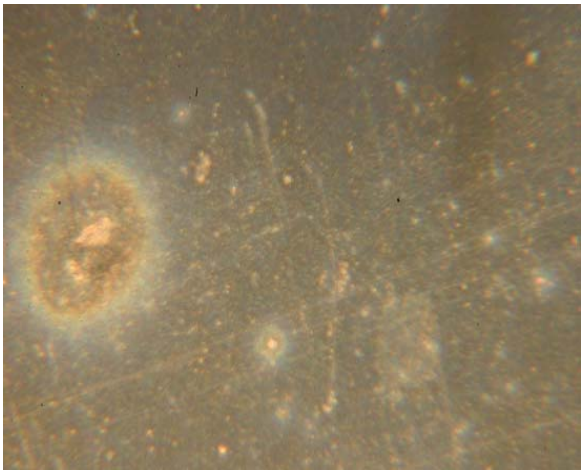

Figure 16: Reacted molybdenum layer (2017R21B)

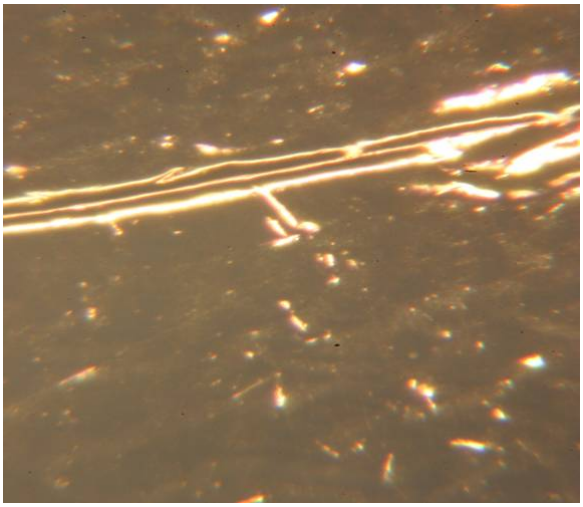

Figure 17: Thermal cracks in molybdenum (2017R21B)

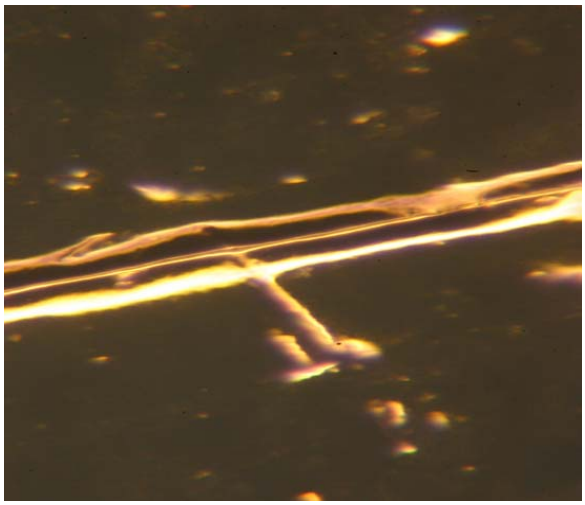

Figure18: thermal cracks in molybdenum (2017R21B)

The optical micrographs reveal various features of the CIGSeS film; most of the film is uniform in appearance as can be seen from figure 15. The molybdenum back contact is getting affected, probably due to reaction with selenium and sulfur (Figure 16) and also thermal cracks are observed in optical micrographs of molybdenum back contacts as examined from the back side through the sodalime glass substrate (Figures 17 and 18).

The scanning electron microscopy results at two different magnifications i.e. 2500X and 5000X are shown in figures 19 and 20; cross-sectional scanning electron microscopy results at magnifications of 18000X and 20000X are shown in figures 21 and 22 respectively.

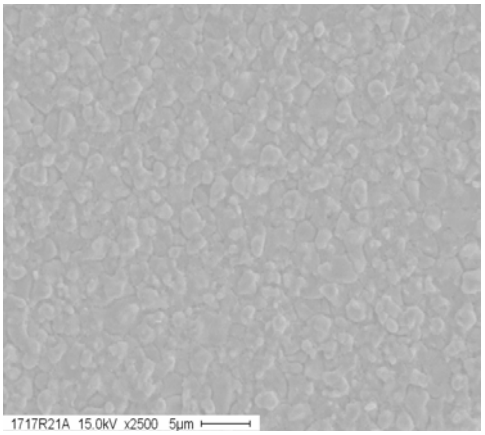

Figure 19: SEM of ~ 2 µm CIGSeS film at 2500X (1717R21A)

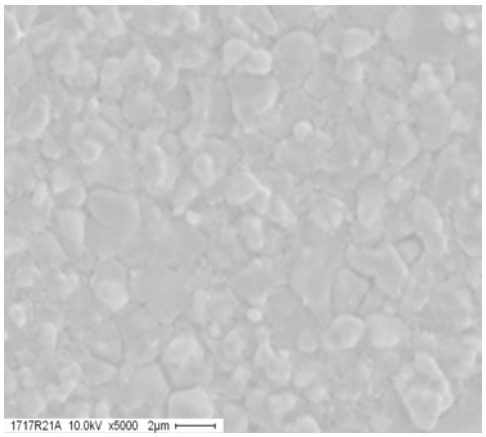

Figure 20: SEM of ~ 2 µm CIGSeS film at 5000X (1717R21A)

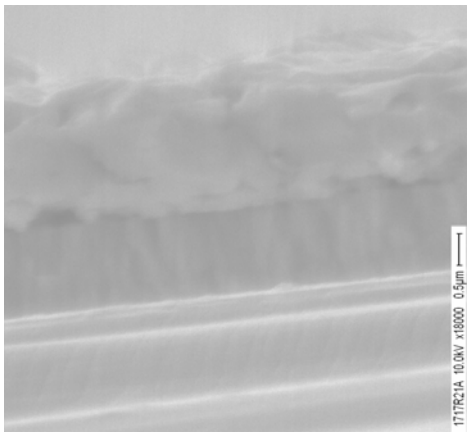

Figure 21: Cross-sectional SEM of CIGSeS µm film at 18000X (1717R21A)

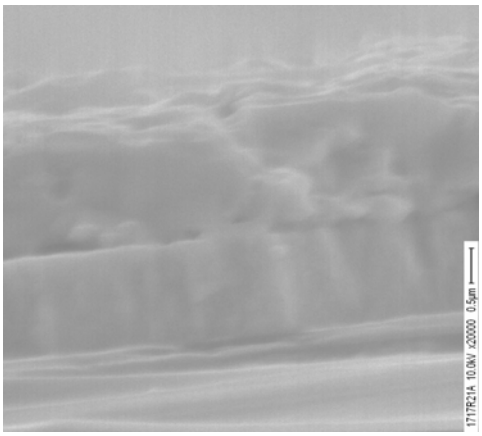

Figure 22: Cross-sectional SEM of ~ 2 CIGSeS film at 20000X (1717R21A)

The SEM micrographs show compactly packed grains with grain size of ~ 2 to 3 microns and the cross-sectional micrographs show CIGSeS film on molybdenum contact with no porosity at the interface, very small grains at the interface are not observed indicating better grain structure.

Cu/In ratio of approximately 1.09 was obtained from XEDS analysis of CIGSeS film indicating a Cu-rich film (Tables III and IV)

Table III: CIGSeS XEDS data

Element	Wt %	At %
InL	32.03	23.26
CuK	19.32	25.37
SeK	48.63	51.63

Table IV: CIGSeS XEDS data

Element	Wt %	At %
InL	33.26	24.17
CuK	20.56	27.00
SeK	46.17	48.8

.

The EPMA results for the CIGSeS films formed on molybdenum coated sodalime glass substrates with no diffusion barrier layer are given in Table V.

Table V: EPMA analysis data for CIGSeS sample prepared by RTP.

Sample ID	Voltage (kV)	Cu	In	Ga	Se	S	Cu/In+Ga	S/Se+S
1317R21U	10	26.68	22.45	2.35	40.53	7.99	1.08	0.16
1317R21U	20	25.52	22.32	3.78	42.61	5.77	0.98	0.12

Cu/In+Ga ratio is being optimized at ~0.80. As can be seen from the EPMA data the Cu/In+Ga ratio obtained was higher, i.e. 0.9776 instead of the range of ~ 0.80. For the above CIGSeS absorber layer, the substrate movement speed during indium sputtering was changed from 41.25 seconds to 5% less, i.e. to 39.4 seconds, rest of the sputtering parameters that is power and pressure were kept same, i.e. 230 watts and 7 x 10^{-4} Torr. As the Cu/In+Ga ratio obtained was higher than required, indium sputtering time was bought back to 41.25 seconds for further experiments.

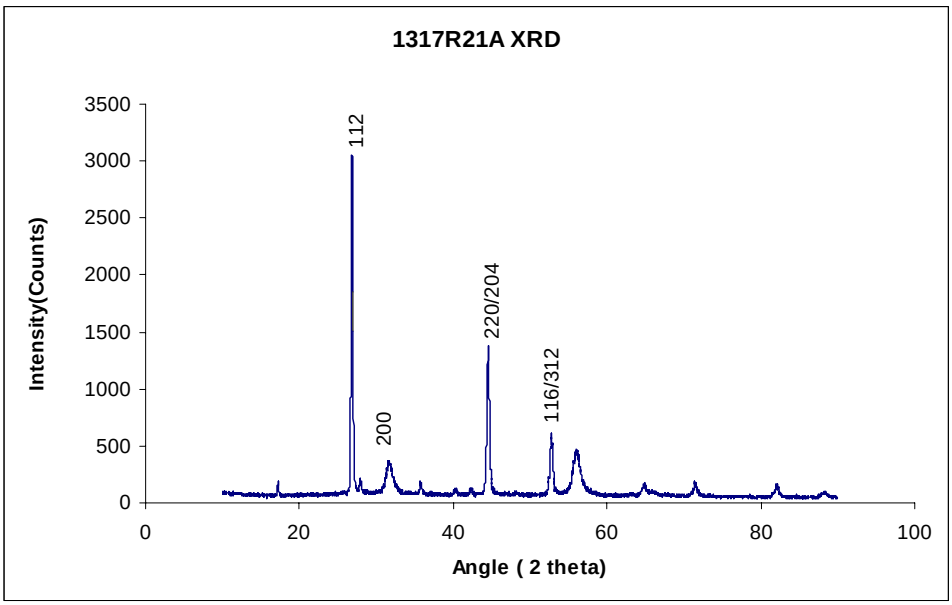

Figure 23: XRD analysis of CIGSeS film.

XRD pattern of sample 1317R21A is shown in figure 23. From the XRD analysis following parameters was calculated: lattice parameter a = 5.758 Å and c = 11.516 Å of the chalcopyrite phase of CIGSeS, giving c/a ratio of 2.000.

Photovoltaic characterization was performed on the cells formed on this absorber layer and the I-V curves were plotted. The PV parameters obtained from this I-V curve are tabulated in Table VI.

Table VI: PV parameters from I-V curve

Sample No.	Cell No.	Cell Area cm^2	V_{oc} mV	I_{sc} mA/cm^2	J_{sc} mA/cm^2	R_s Ω	R_p Ω	FF %	η %
1317R21E	01	0.441	400	6.65	15.08	80	700	53	3.2

Due to high series resistance R_s the short circuit current density J_{sc} value is relatively lower; one of the reasons for higher R_s is that molybdenum back contact is getting affected.

The thermally affected and cracked molybdenum back contact is also being studied further to improve the series resistance of the cell.

External QE, LBIC and C-V analysis was carried out on the 12.78% efficient cell at Colorado State University (CSU) and the results are provided in the following.

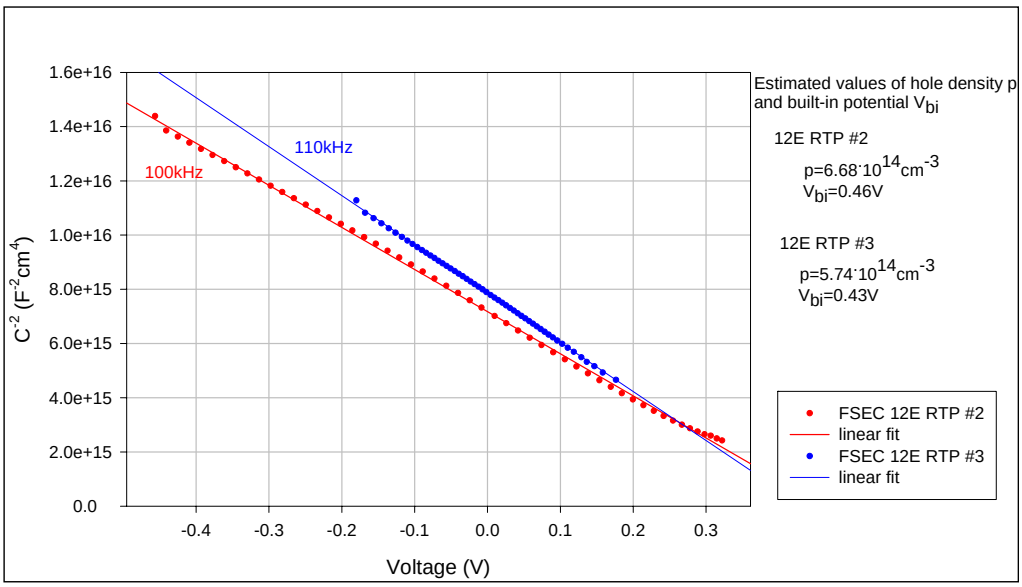

Figure 24: C-V Plot for RTP 12E

Figure 24 shows C-V measurements from substrate12E RTP. The data is fairly clean, and the C^{-2} vs V plots are reasonably linear with plausible voltage intercepts. The inferred hole densities are all in the higher mid-10^{14} range and modest variation between cells on the same substrate.

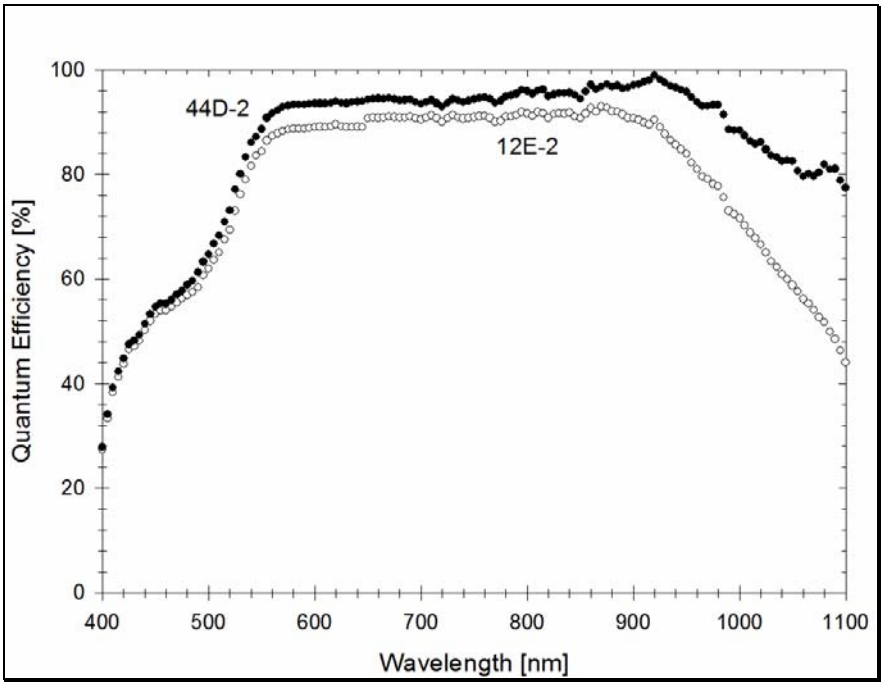

Figure 25: External QE Analysis

External QE analysis (Figure 25) of 12E RTP shows a band gap about 1.1 eV.

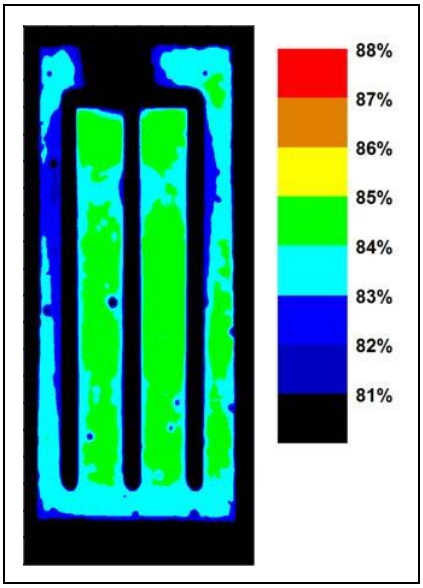

Figure 26: LBIC photoresponse map of RTP 12E-2

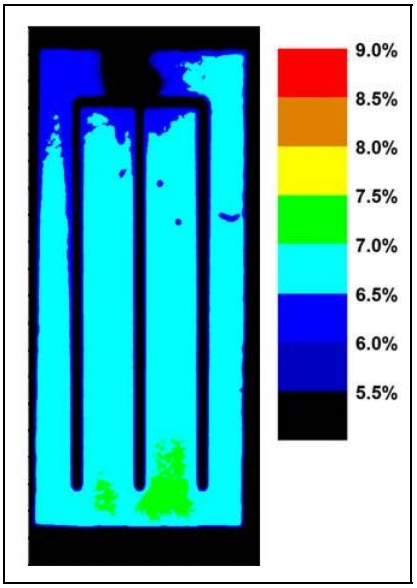

Figure 27: LBIC photoresponse map of RTP 12E-7 Shunted

Figures 26 and 27 show that LBIC photoresponse (QE) maps for the same cells (one shunted and one not). Part of the dark area at the top is the probe shadow. Absolute QE is clearly a factor of 10 to 20 less for the shunted cells. Also the shunted pattern spreads gradually over the entire cell, which is typical.

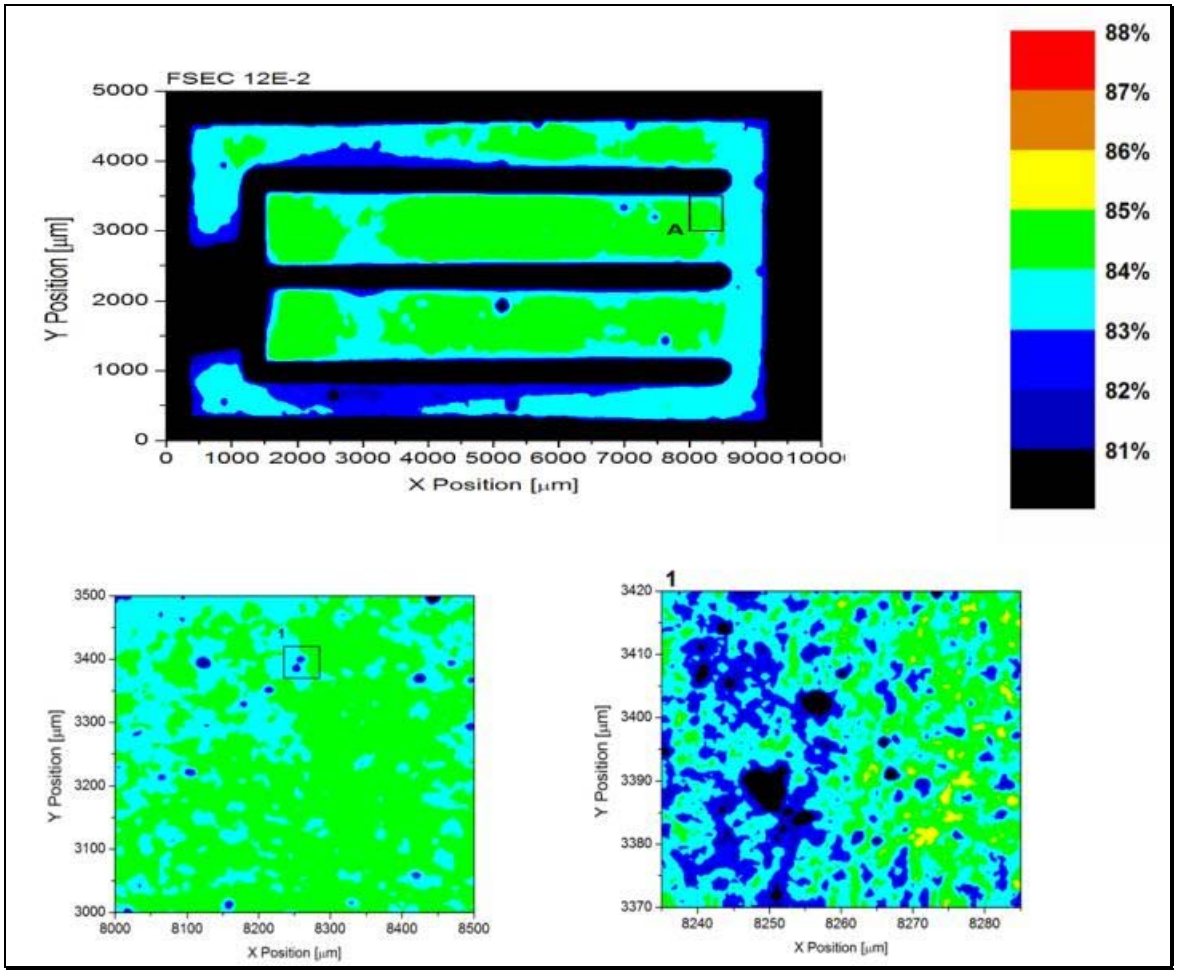

Figure 28: LBIC photoresponse map of RTP 12E-2

Figure 28 (12E RTP) rotate the non-shunted maps 90º, and enlarge the regions shown by squares first ten times (A) and then another ten times (1), with corresponding reductions in probe dimension (100 µm, 10 µm, and 1 µm). The probe intensity was held near one sun for all of the LBIC measurements.

4. **CIGS2 THIN FILM SOLAR CELLS**

Chalcopyrite structure CIGS2 thin films are being extensively considered for use in high-efficiency photovoltaic cells. At FSEC PV Materials Laboratory, record efficiency of 11.99% has been achieved on a 2.7 μm CIGS2 film prepared by sulfurization [4]. Recent research endeavors in the CIGS2 thin film photovoltaic community are directed towards thinner films because the availability and cost of Indium are limiting factors [5]. The required amounts of metals can be lowered by using thinner films. Initially, small sized grains are formed during the film growth [6]. With continuing growth to larger thicknesses, more favorably oriented grains grow faster at the expense of others and coalesce to form compactly packed large-grain morphology. Hence certain minimum thickness of a thin film may be essential for the grains coalesce and grow. The solar cell performance in smaller grained chalcopyrite absorber deteriorates due to detrimental effects of the larger fraction of grain boundaries [7]. It is essential to hasten the grain growth through coalescence to retain high-quality properties even in thinner films. Large grain size that is desirable for obtaining high efficiency cells can be achieved by creating conditions of fewer nucleation sites and large mobilities of the deposited species. There are limits to employing very high temperature processing for increasing the mobility because of the softening temperature of the sodalime glass and excessive reaction of sulfur carrying precursors with the molybdenum back contact. Sodium may play a vital role by enhancing the atomic mobility and improving the coalescence even in thinner films; sodium incorporated CIS2 films have already shown better device properties and increased p-type conductivity [8, 9]. It will be interesting to study if sodium can play a role in copper-poor CIGS2 absorbers also. In copper-rich CIGS2 precursors, increased mobility and consequently absorber phase formation is obtained due to liquid-like behavior of pseudo-binary phase region $Cu_{2-x}S$. Hence sodium may not play a vital role in copper-rich precursors. Copper-rich precursors for this purpose are prepared with excess copper. After sulfurization, the absorber film is etched to remove the $Cu_{2-x}S$ layer segregating at the surface. This would lead to the stoichiometric Cu/In+Ga of unity but not to the desired Cu-poor composition for attaining optimum doping level. This also makes the film rough. Copper-poor absorber can produce a comparatively smooth film and better morphology. This work presents a study of morphology and device properties of CIGS2 thin films with copper-poor absorbers after minute amounts of sodium are introduced on the Mo-coated substrate in the form of sodium fluoride layer prior to sputter deposition of copper, indium and gallium. The amount of sodium varied systematically. Three different thicknesses of NaF were chosen: no NaF, 40 Å of NaF and 80 Å of NaF respectively. NaF was deposited by thermal evaporation on molybdenum coated glass samples. Subsequently CIGS2 thin films were prepared in two stages. Stage one involved the deposition of slightly copper-poor CuGa-In metallic precursors on molybdenum coated glass substrates. Stage two involved the sulfurization of these metallic precursors in dilute H_2S (4-8% H_2S) ambient. One part of each sample was etched in a 10% KCN solution, while one part was kept unetched. This was followed by further deposition steps in order to complete the cell. Scanning electron microscopy (SEM) was performed using a scanning electron microscope model JEOL 6400 F. Current-voltage (I-V) characteristics and optical microscopy were performed at the FSEC PV materials laboratory.

Optical microscopy

Large density of hillocks was observed in the sample without NaF at 500 X as shown in Figure 29. These hillocks were uniformly spread all over the sample. These features were retained to some extent in the sample with 40 Å NaF (Figure 30), the shape was different than those seen in Figure 29 and here the features looked like protrusions out of a uniform film. The sample with 80 Å NaF contained no predominant features (Figure 31).

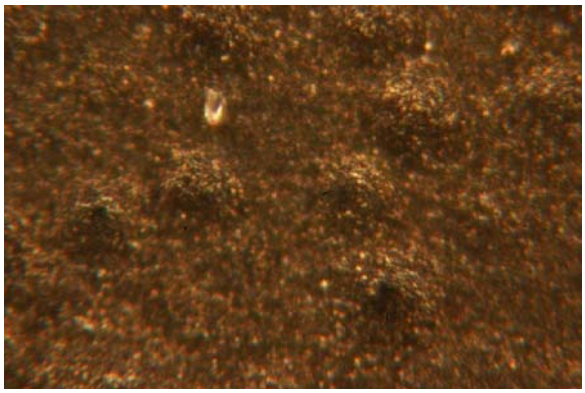

Figure 29: Sample without NaF at 500 X.

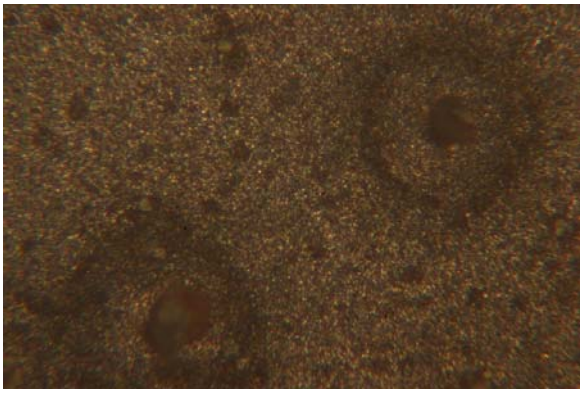

Figure 30: Sample with 40 Å at 500 X.

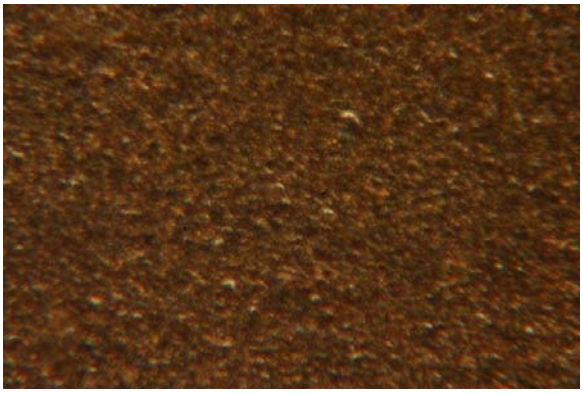

Figure 31: Sample with 80 Å at 500 X.

Scanning electron microscopy

Scanning electron microscope showed features similar to those observed by optical microscopy. The sample without NaF contained predominant hillock shaped features on the background of a uniform grain structure (Figure 32), whereas the sample with 80 Å NaF contained no predominant features and uniform grain structure was observed as shown in figure 33.

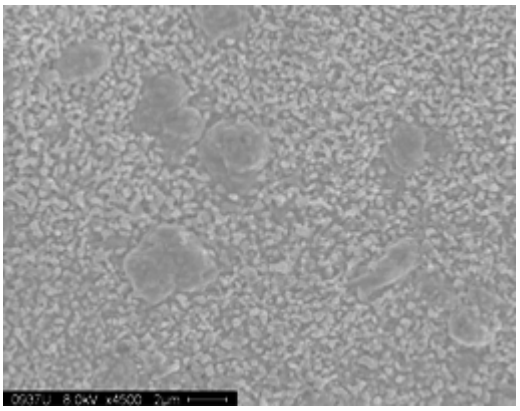

Figure 32: Sample without NaF at 4500 X.

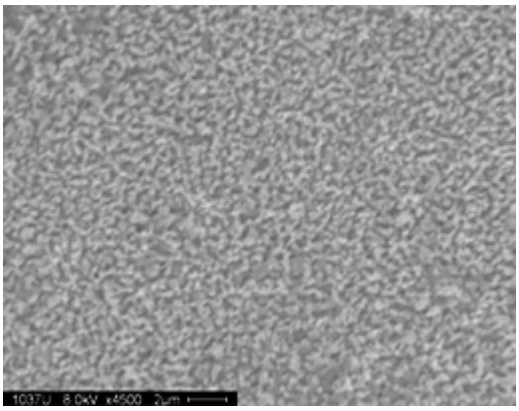

Figure 33: Sample with 80 Å at 4500 X

Current-voltage characteristics

Photovoltaic conversion efficiencies were calculated using current-voltage (I-V) characteristics. The efficiency data is summarized in Table I for unetched and etched samples of all three types. It is observed that the efficiencies are typically higher in all etched samples than their unetched counterparts. This is due to the excess $Cu_{2-x}S$ layer forming above CIGS2 layer. Addition of NaF is also found to enhance the efficiencies. Highest efficiency of 3.46 % is obtained in the sample with 80 Å NaF. Unetched sample without any NaF addition has comparatively better efficiencies than with NaF samples; also etching does not do much difference for the sample without NaF. These results (Table VII) are preliminary and more work is being carried out.

Table VII. Efficiency table (in percentage).

Sample	No NaF	40 Å	80 Å
Unetched	*2.34*	*0.81*	*1.36*
etched	*2.38*	*2.55*	*3.46*

CONCLUSIONS

Addition of NaF and etching by KCN produced better results in Cu-poor CIGS2 precursors. Further experiments will be carried out with varying degrees of NaF to study its effect in detail. There seems to be segregation of some Cu-rich phase after sulfurization which appears as hillocks in the micrographs, after etching there is improvement in performance. Sodium also seems to be playing a vital role in the improvement in performance.

5. ZnCdS AND ZnS AS ALTERNATIVE BUFFER LAYER FOR CIGS2 SOLAR CELLS

CdS heterojunction partner layer has shown high photovoltaic conversion efficiencies with CIGS absorber layer while efficiencies are lower with $CuIn_{1-x}Ga_xS_2$ (CIGS2) absorber layers due to high conduction band offset that result in lower values of open circuit voltage and higher interface recombination [10]. Devices with ZnS heterojunction partner layer have shown better blue photon response due to a higher bandgap as compared to devices with CdS heterojunction partner layer [10, 11]. Moreover, it has been predicted that lower conduction band offset and higher efficiency may be achieved for cells with alternative buffer layer such as ZnS and ZnCdS. Therefore, a comparative study, of ZnS, ZnCdS and CdS was carried out to study the advantages and applicability of ZnS and ZnCdS as heterojunction partners for CIGS2 devices. Better lattice match of ZnS and ZnCdS with CIGS2 can lead to reduced interfacial recombination resulting in higher voltages. This increase in currents and voltages can result in higher efficiencies as compared to those obtained for CdS/CIGS2 devices. Materials characterization was carried out on the samples to understand the chemical compositions of n-type heterojunction partners. Photovoltaic characterization was also carried out to observe the photovoltaic parameters of the completed devices.

Experimental

The absorber film was fabricated by sulfurization of metallic precursors (CuGa and In) deposited by DC magnetron sputtering in Cu rich regime (Cu/(In+Ga)>1). $Cu_{2-x}S$ phase that segregates at the surface was etched away using a dilute KCN solution before the deposition of heterojunction partners by chemical bath deposition (CBD). i:ZnO/Al:ZnO window bilayer was deposited by RF sputtering, finally contact fingers of Cr/Ag were deposited by thermal evaporation through a mechanical mask.. ZnS/CdS/CdZnS depositions were carried out in an aqueous solution of $ZnSO_4$ or/and $CdSO_4$, NH_4OH, and $SC(NH)_2$ in a chemical bath. Various thicknesses were obtained by varying the deposition time. SnO_2:F deposited glass was used as substrates for preparing samples for optical spectroscopy. The transmission and reflection optical spectra were carried out with a UV-VIS Recording Spectrophotometer. X-ray photoelectron spectroscopy was carried out for chemical analysis and to determine atomic ratios. X-ray diffraction (XRD) was carried out to determine the crystallographic structure of the film. Current-voltage characteristics of completed cells were taken under simulated AM1.5 at 25° C.

Initially optimization of concentrations for various chemical reagents was carried out, and its effect on thickness and composition of film is studied. The substrate used for initial studies was fluorine doped SnO_2 coated sodalime glass. Initially aqueous solution of zinc sulfate/cadmium sulfate was added in an organic solvent and then aqueous solution of ammonium hydroxide and thiourea were subsequently added to the solution. The substrate was then dipped in this solution and reaction was carried out for 45 minutes. Temperature of the solution was maintained at between 75° C -80° C throughout the process. Various deposition parameters were used to deposit ZnCdS layer, bath parameters for ZnCdS deposition reported elsewhere [2] seems to be nearly optimized for this system. CBD ZnCdS was prepared using 0.0002 M CdSO4, 0.02 M of ZnSO4, 0.58 M ammonia, and 0.25 M thiourea dissolved in a

mixture of water and organic solvent. Further studies are needed to fine tune it. For ZnS deposition bath parameters are yet to be optimized.

Results

With initial bath parameters the cell efficiencies below 2% were obtained, and optical transmittance/ X-ray diffraction studies indicated that the film was too thin. With the bath parameters reported elsewhere [11], efficiencies comparable to cells with CdS as heterojunction partner were obtained. Therefore, results for near optimized heterojunction partner is discussed in this report.

The near surface composition of ZnS and ZnCdS films deposited on CIGS2 samples was characterized by X-ray photoelectron spectroscopy studies The XPS analysis was carried out using Physical Electronics 5400 ESCA equipped with Mg K_α X-ray source and results are shown in figure 34, 35 and 36.

The measured XPS spectra were shifted to match carbon peak to the binding energy of 284.6 eV so as to eliminate the charging effects. XPS spectra of CBD ZnCdS layers showed peaks of Cd $3d_{5/2}$, $Zn2P_{3/2}$, $S2P_{3/2}$ at approximately 405.1 eV, 1022.5 eV and 161.4 eV respectively. Peaks of CdS, CdO_2 and $Cd(OH)_2$ were observed in $Cd3d_{5/2}$ core level spectra while the peaks of ZnS, ZnO and $Zn(OH)_4$ were observed in $Zn2p_{3/2}$ core level spectra. $Zn2P_{3/2}$, and $S2P_{3/2}$ peaks were observed in the case of ZnS layers.

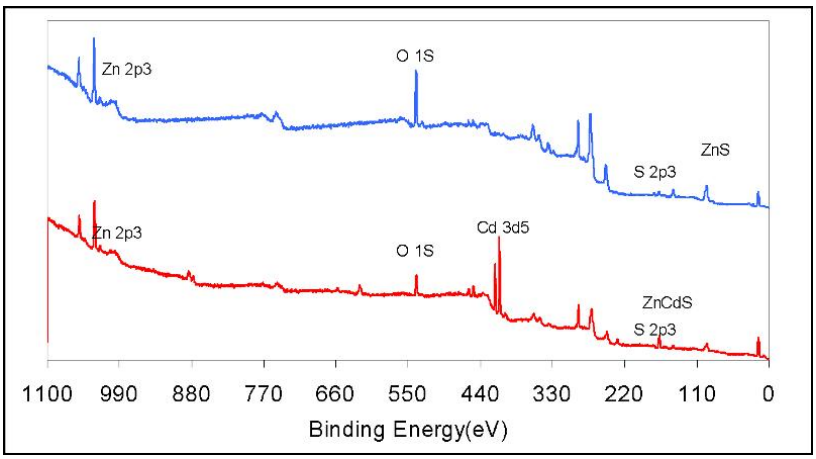

Figure 34: XPS spectra for ZnS and ZnCdS thin films deposited on CIGS2 film.

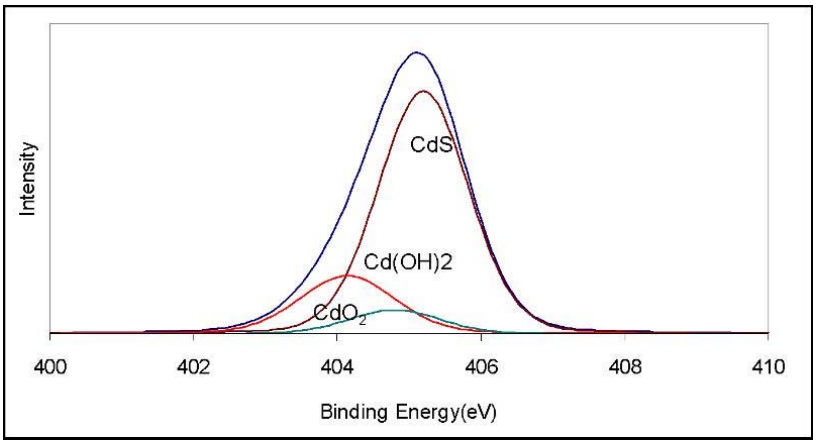

Figure 35: Cd $3d_{5/2}$ peak in the XPS spectrum of a CdZnS layer. Curve fitting to show contribution of CdS, $Cd(OH)_2$ and CdO_2 peaks to corresponding XPS peak is also plotted.

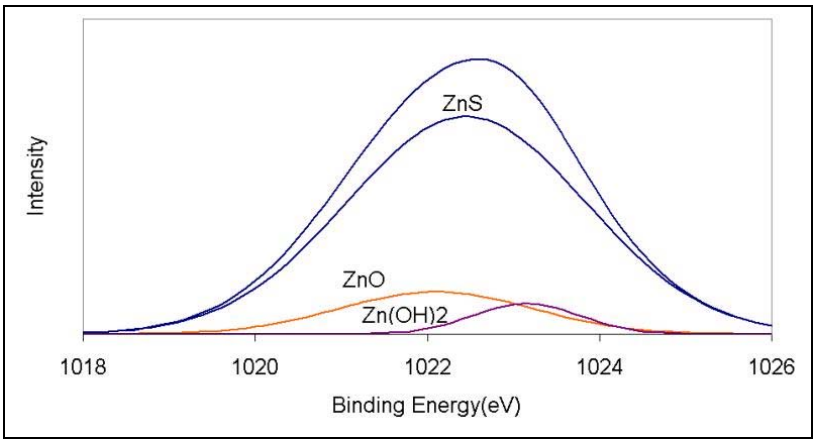

Figure 36: Zn $2p_{3/2}$ peak in the XPS spectrum of a CdZnS layer. Curve fitting to show contribution of ZnS, $Zn(OH)_2$ and ZnO peaks to corresponding XPS peak is also plotted.

XRD patterns of ZnS/ZnCdS films deposited on SnO_2:F coated glass did not show any discernible peaks of ZnS layer indicating that film was too thin. XRD pattern of ZnCdS deposited on SnO_2:F coated glass showed only broad peaks indicating that the film was amorphous (Figure 37). Optical transmission spectra shows lower absorption for ZnCdS films as compared to CdS layer as deposited ZnCdS layer was thinner (Figure 38). Steeper drop in transmittance for CdS is observed for lower wavelengths as compared to ZnCdS layer due to lower bandgap of CdS. Therefore, the transmittance of ZnCdS layer is higher at all wavelengths than that of CdS layer. Moreover, the optical spectrum of ZnCdS layer does not show the substantial absorption above the CdS band edge. For ZnS layer transmittance is still higher however as indicated by XRD studies this film is too thin.

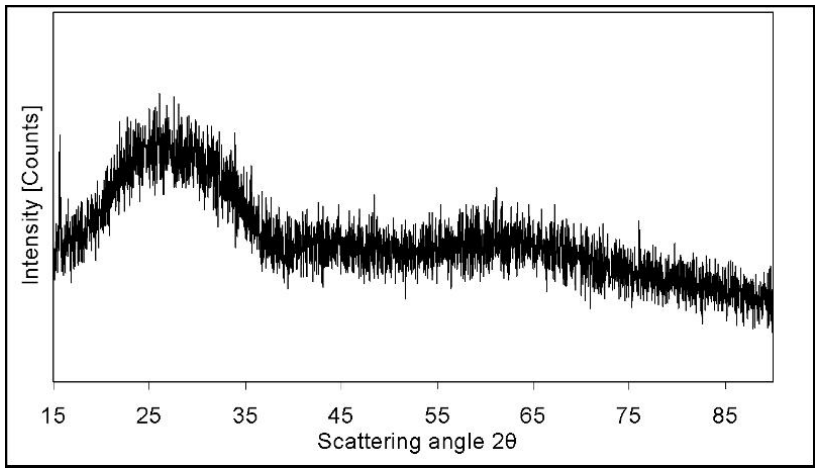

Figure 37: X-ray diffraction pattern of as ZnCdS film deposited on tin oxide coated glass substrate.

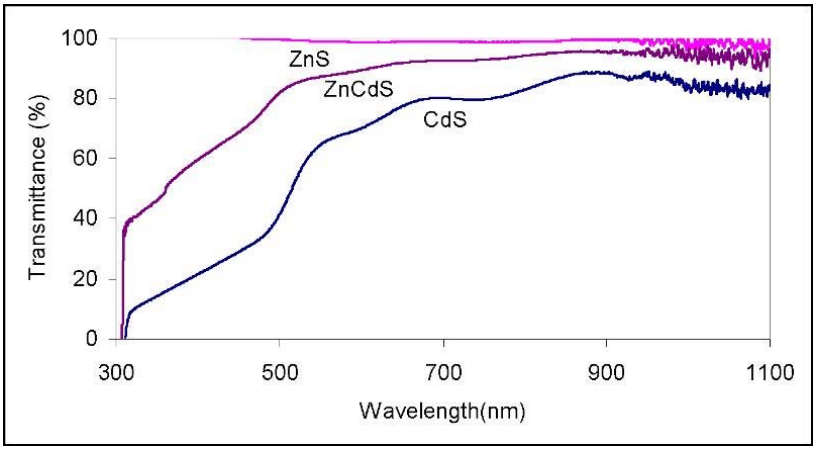

Figure 38: Optical transmittance spectra for films deposited on tin oxide coated glass

The J-V characteristics of completed cells with varying deposition time for ZnCdS and control cell CIGS2/CdS are shown in Figure39. Cells with ZnCdS as heterojunction partner have shown higher short circuit current density. This can be attributed to better blue photon response due to higher bandgap of ZnCdS as compared to CdS. ZnCdS with deposition time of 30 minute have given best cell with efficiency of 4.9%. These are only preliminary results and further experiments are planned. Solar cell parameters are tabulated in Table VIII. Even with higher efficiency for ZnCdS, the series and shunt resistance obtained with ZnCdS is 341 Ω and 791 Ω respectively compared to those obtained with CdS, 31.5 Ω and 2233 Ω respectively. It would be essential to improve these parameters so as to achieve high efficiency cells with ZnCdS.

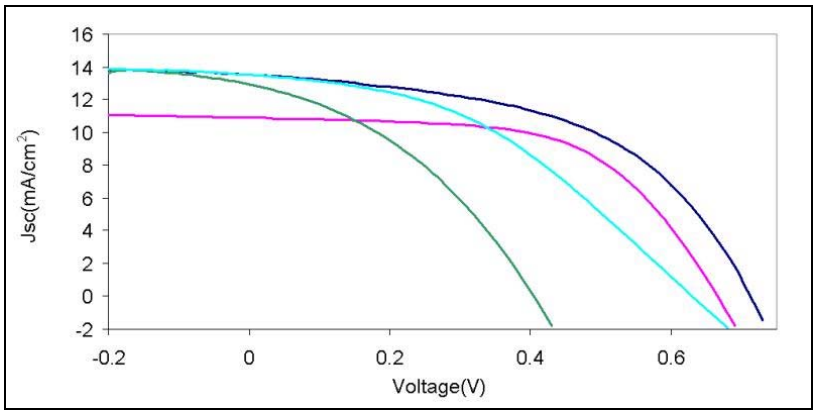

Figure 39: The J-V characteristics for CIGS2/ZnCdS for deposition time of 15, 30 and 40 minutes respectively and CIGS2/CdS solar cells under AM 1.5 condition

Table VIII. Solar cell parameters of CIGS2/CdZnS for various deposition time and for control cell CIGS2/CdS thin film solar cell

	ZnCdS			**CdS**
Deposition time(min)	15	30	40	
V_{oc} (V)	0.4	0.7	0.63	0.66
FF (%)	38.3	51.9	41.29	56.3
Efficiency, η (%)	2.0	4.9	3.5	4.44
J_{sc} (mA/cm^2)	12.9	13.5	13.50	11.98

CONCLUSION

High current values can be attained using ZnCdS as the heterojunction partner for CIGS2 solar cells hence higher conversion efficiencies can be realized. Series and shunt resistance need to be improved so as to improve the efficiency of these solar cells. The effect of better lattice match needs to be further investigated. Deposition conditions for ZnS layers need to be further optimized. CIGS2 absorber needs to be further optimized to make any conclusive comment.

6. ULTRA THIN CIGS/CIGSS ABSORBER LAYER

Several features similar to ones observed on thicker CIGS films and as reported in earlier reports were observed on very thin CIGS absorber films (1747T8B) too. Figure 40 shows the optical images of the features. Features such as whiskers and globules were observed. Some modifications were carried out during the selenization of the metallic precursors. After these modifications, density of these features reduced drastically and an overall uniform film (2147T8C) was obtained as can be seen in figure 41.

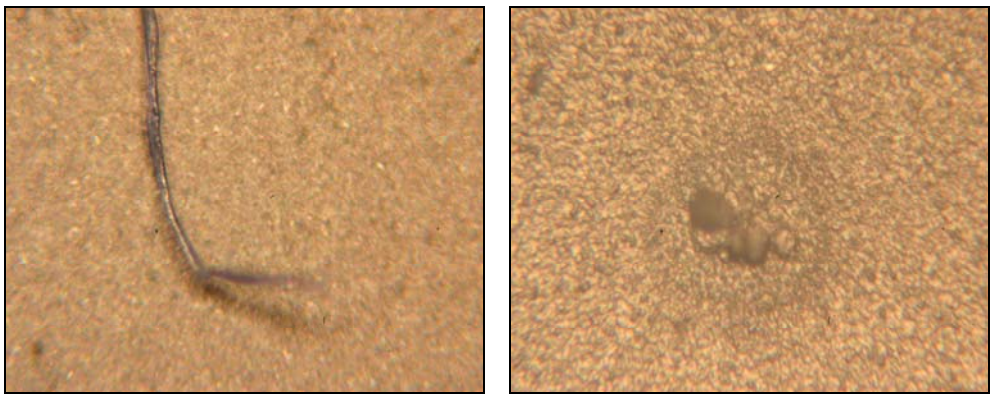

Figure 40: Some of the features observed on sample 1747T8B

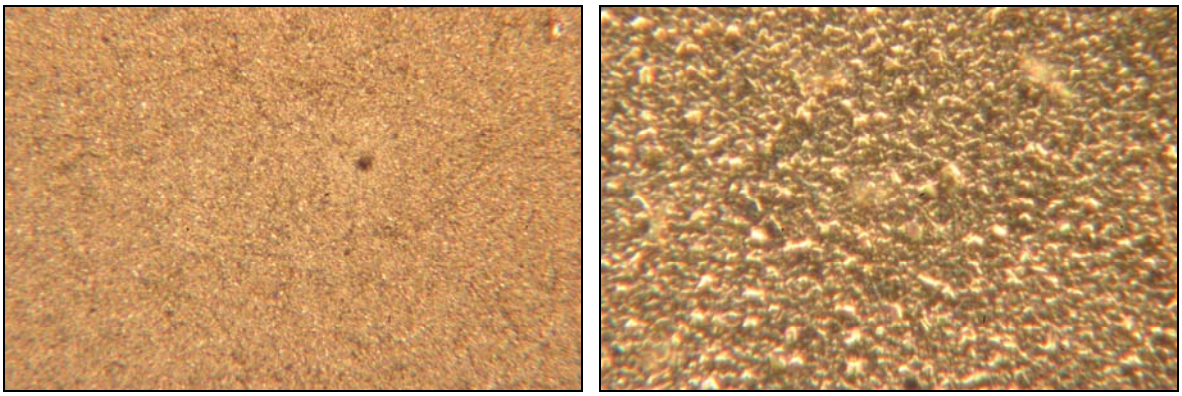

(a) (b)

Figure 41: Optical Images of sample 2147T8C (a) 100 X magnification (b) 500 X magnification

Scanning electron microscopy (SEM) of the two samples was carried out and is shown in figures 42 and 43. Grain size of <1 μm is observed in the film which was grown in horizontal position where as slightly larger grains were observed in case of sample placed vertically. Fairly faceted structure is observed in both the films. However, large density of smaller grains is also observed thus increasing the volume of grain boundaries.

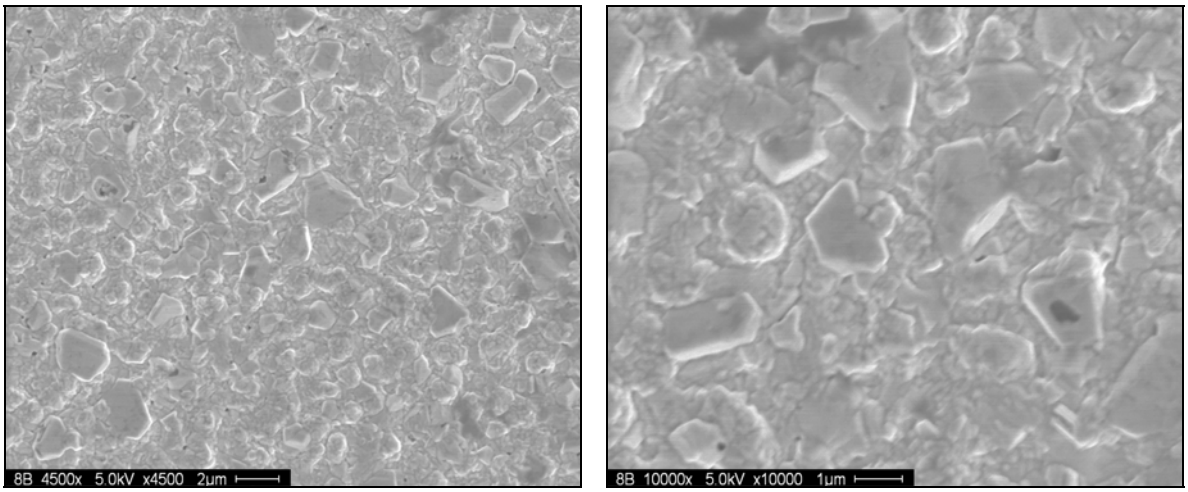

(a) (b)

Figure 42: SEM images of sample 1747T8B (a) 4500X Magnification (b) 10000X Magnification

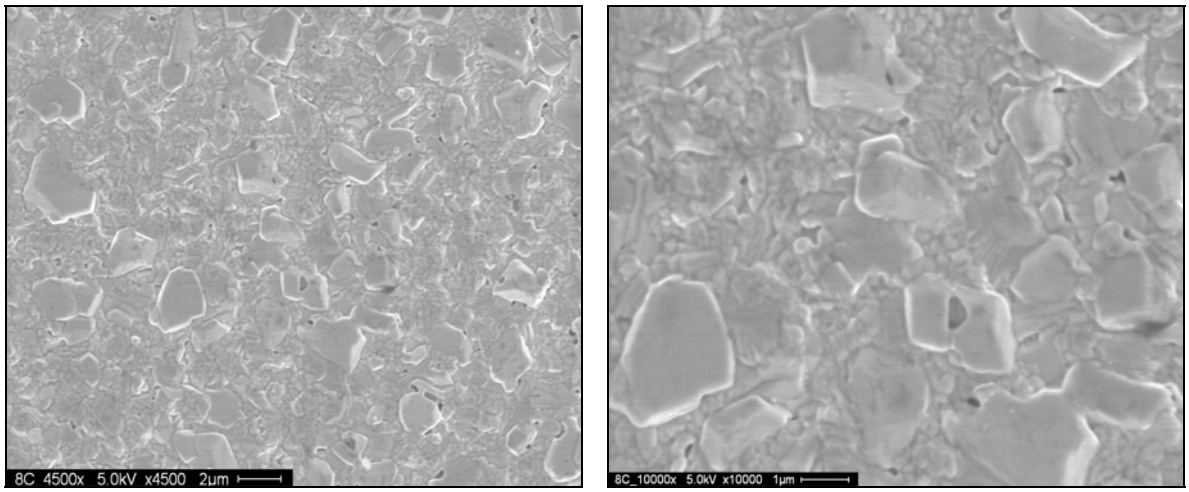

(a) (b)

Figure 43: SEM images of sample 2147T8C (a) 4500X Magnification (b) 10000X Magnification

During this year, substrates that were conventionally used were changed. Earlier Mo coated sodalime glass with barrier layer were used and now the substrates were Mo coated sodalime glass but without the barrier layer. Since the barrier layer was not used to avoid the out diffusion of sodium from the sodalime glass experiments were carried out to optimize the amount of additional sodium that needs to be present during the selenization of the precursors. Further experiments need to be carried out for optimizing the additional amount of sodium.

Further experiments will be carried out to optimize the selenization time-temperature profile for very thin CIGS absorber films. This is necessary because lower temperature reduces the grain size and too higher temperature affects the Mo back contact thus increasing the series resistance.

7. MAINTENANCE AND REPAIR OF VACUUM SYSTEMS

Cryopumps Maintenance

Cryopumps are used to obtain vacuum in the sputtering chambers used for metaalic precursors and ZnO:Al doped deposition. Two cryopumps are used in the sputtering chambers, a larger cryopump is used for obtaining vacuum in CuGa and In, DC magnetron sputtering chamber and smaller cryopump is used for obtaining vacuum in i-ZnO and ZnO:Al RF magnetron sputtering chamber.

Maintenance of these pumps became essential because the ultimate vacuum level obtained in the chambers was deteriorating and it was necessary to carry out frequent regeneration for these cryopumps. Therefore, maintenance kits for both the cryopumps were ordered and procured. After this, the smaller cryopump was dis-assembled for inspection and thoroughly cleaned. Coldhead and displacer assembly O-rings and gaskets that are subjected to wear during service were replaced with new O-rings and gaskets from the service-kit. After replacing the worn-out components and reassembling the displacer, was kept in oven for baking at 80°C for 24 hours. After this step, the displacer assembly was reassembled into the cryopump.

It was decided to replace absorber in the compressor since it was nearing the completion of service life period of 15000 hours. A new cryocompressor cryodrive absorber unit was been procured and was installed in the cryocompressor. The cryocompressor was re-charged with helium to obtain earlier level helium pressure of 16.5±1.0 bar.

The smaller cryopump was connected to the cryocompressor using helium lines and the pump down was initiated. A low temperature of ~20 K was obtained in the cold head.

The same maintenance procedure was repeated for the larger cryopump unit and after successfully completing the maintenance procedure, both the cryompumps were connected in parallel to the cryocompressor. Now the cryopumps are being used for obtaining vacuum of the order of 10^{-6} Torr in CuGa and In DC magnetron sputtering chamber and the i-ZnO/ZnO:Al RF magnetron sputtering chamber. With the completion of maintenance of the cryopumps and cryocompressor, sputtering of CuGa and In metallic precursors and i-ZnO/ZnO:Al window bilayer is being carried out routinely.

Diffusion Pump Maintenance

During the fabrication of CIGSeS thin film solar cells some of the processes are carried out by vacuum evaporation. These processes include sodium fluoride (NaF) deposition for incorporation of controlled amount of sodium in the CIGSeS film, elemental selenium deposition during CIGSeS formation by rapid thermal processing (RTP) and, deposition of chromium and silver contact fingers.

Vacuum in the evaporation chamber is obtained by mechanical pump and diffusion pump. Initial vacuum in diffusion pump is obtained by mechanical pump using backing valve. This backing valve is in turn activated with the help of pneumatic driven solenoid valve actuator. During a deposition process, the solenoids valve actuator malfunctioned and the backing valve did not open. Due to this the diffusion pump oil backstreamed into the vacuum evaporation chamber. During the maintenance period, all regular experiments were temporarily halted, a new

pneumatic driven solenoid valve was procured and all the vacuum evaporation systems components were disassembled for thorough cleaning.

The system components that were disassembled for cleaning included diffusion pump, liquid nitrogen trap, gate valve, backing and roughing valves and, vacuum evaporation chamber components e.g. electrodes and substrate mounting mechanism parts. These components were individually dismantled, so that all the inside surfaces could be cleaned properly. The initial cleaning was carried out by lint free cloth to wipe out the oil. Then these parts were thoroughly cleaned with the help of soap and high pressure water jet. Afterwards these parts were degreased to insure that no traces of oil remained. The inside surface of the vacuum evaporation chamber was also thoroughly cleaned using the same procedure. All the components were thoroughly dried for 24 hours in air to insure effective moisture removal. For intricate parts the drying was also facilitated using a hot air blower.

The individual components e.g. liquid nitrogen trap, gate valve, backing and roughing valves were then reassembled. As the diffusion pump oil has backstreamed into the chamber, the quantity of the oil in the diffusion pump was reduced. New diffusion pump oil was refilled to ensure that the oil quantity was back to normal level i.e. 800 ml. These components were mounted back into the system and their pneumatic, electrical and cooling water connections were carried out. After this the system was tested and normal operation was observed. Currently the vacuum evaporation processes are resumed in a routine manner.

Mechanical Pump Maintenance

The CIGSeS thin films are prepared by depositing CuGa-In metallic precursors on molybdenum coated glass substrates by using DC magnetron sputtering, after selenization/sulfurization and CdS heterojunction partner layer deposition on CIGSeS layer, the next step is to carry out ZnO/ZnO:Al window bilayer deposition by RF magnetron sputtering. The systems are pumped by combinations of cryopumps and mechanical vacuum pumps. After the maintenance of the cryopumps it was also observed that the pump down rate of the mechanical pump had deteriorated and maintenance of the mechanical pump was required.

The maintenance kit and krytox oil for this mechanical pump were procured for this reason. Once the maintenance of the pump was carried out the initial pumping down of the sputtering chambers was back to normal. With the completion of maintenance of the mechanical pump, sputtering of CuGa and In metallic precursors and i-ZnO/ZnO:Al window bilayer are being carried out routinely.

Substrate Moving Mechanism

During the sputtering of the metallic precursors and the window layer the substrate is moved at constant speed over the sputter targets to obtain uniform thickness of the film. Due to heavy use and general wear and tear the connector feed-through connecting the stepper motor to the rotating shaft in the system for deposition of the i-ZnO/ZnO:Al window bilayer was damaged. A new feed-through was procured. It was also observed that the rotating shaft and the stepper motor fixture were misaligned. They were aligned. Similar issues were observed in the case of the system for deposition of molybdenum and CuGa-In metallic precursors. Necessary corrections were made to this fixture too. After fixing up the substrate moving mechanism in both the sputtering chambers, routine depositions were resumed.

8. REFERENCES

1. T. Wada, N. Kohara, S. Nishiwaki, T. Negami, "Characterization of the Cu(In,Ga)Se_2/Mo Interface in CIGS solar cells", Thin Solid Films Vol. 387, 2001, pp. 118-122
2. D. Ras, D. Mukherji, G. Kostorz, D. Brémaud, M. Kälin, D. Rudmann, M. Döbeli, and A. Tiwari, "Dependence of the $MoSe_2$ Formation on the Mo Orientation and the Na Concentration for Cu(In,Ga)Se2 Thin-Film Solar Cells", Mater. Res. Soc. Symp. Proc. Vol. 865, F8.1
3. High Throughput, Low Toxic Processing of Very Thin, High Efficiency CIGSS Solar Cells, Year 1, Final Report.
4. Jahagirdar A. H., Kadam A. A. and Dhere N.G., IEEE 4th World Conference on Photovoltaic Energy Conversion, Hawaii, pp. 557-559, 2006.
5. I.Luck, J.Kneisel,K.Siemer,J.Bruns,R.Scheer,R.Klenk,N.Janke and D.Braunig, Solar Energy Materials & Solar Cells, Vol.67 , pp. 151-158, 2001.
6. T. Yamamoto, K.Fukuzaki and S.Kohiki, Applied Surface Science, Vol. 159-160, pp. 345-349, 2000.
7. B.A. Anderson, C. Azar, J.Holmberg and S.Karlsson, Energy 1998;23(5): pp.407-411.
8. J. L. Vossen, and W. Kern., “Thin film processes”, Newyork academic press, 1978.
9. K. Taretto, U. Rau, J. Werner; Thin Solid Films, 2005:Vol. 480-481, pp. 8-12.
10. M.A.Contreras, T.Nakada, M.Hongo, A.O.Pudov, J.R.Sites, ZnS(O,OH)/Cu(In,Ga)Se2 solar cell with 18.6% efficiency. In: 3rd World Conference on Photovoltaic Energy Conversion, Osaka, Japan, May 2003.
11. R.N.Bhattacharya,K.Ramanathan,L.Gedvilas,B.Keyes Cu(In,Ga)Se2 thin-film solar cells with ZnS(O,OH), Zn–Cd–S(O,OH), and CdS buffer layers. Journal of Physics and Chemistry of Solids 66(2005) 1862–1864.